AGU PUBLICATIONS

JGR

Journal of Geophysical Research: Space Physics

RESEARCH ARTICLE
10.1002/2017JA024491

Key Points:
- Electron pitch angle distributions are used to determine magnetic topology at Mars
- Electron voids and trapped distributions indicate closed topology, found more frequently near crustal sources and at lower altitudes
- Trapped distributions become more frequent in crustal fields as they move from dusk to dawn across the nightside

Correspondence to:
T. Weber,
tristan.weber@colorado.edu

Citation:
Weber, T., Brain, D., Mitchell, D., Xu, S., Connerney, J., & Halekas, J. (2017). Characterization of low-altitude nightside Martian magnetic topology using electron pitch angle distributions. *Journal of Geophysical Research: Space Physics*, *122*. https://doi.org/10.1002/2017JA024491

Received 19 JUN 2017
Accepted 9 SEP 2017
Accepted article online 14 SEP 2017

Characterization of Low-Altitude Nightside Martian Magnetic Topology Using Electron Pitch Angle Distributions

Tristan Weber[1], David Brain[1], David Mitchell[2], Shaosui Xu[2], Jack Connerney[3], and Jasper Halekas[4]

[1]Laboratory for Atmospheric and Space Physics, University of Colorado Boulder, Boulder, CO, USA, [2]Space Science Laboratory, University of California, Berkeley, CA, USA, [3]Goddard Space Flight Center, Greenbelt, MD, USA, [4]Department of Physics and Astronomy, University of Iowa, Iowa City, IA, USA

Abstract Magnetic field lines at Mars act as direct pathways for both energy inflow and ion escape. Local variations in magnetic field topology can therefore directly impact the interaction between the solar wind and the Martian ionosphere. One method of analyzing magnetic topology is through the use of electron pitch angle distributions (PADs). Previous PAD investigations have characterized magnetic topology in the Martian system using data from the Mars Global Surveyor spacecraft, but these studies were orbitally constrained to ~400 km altitude and 2 a.m./2 p.m. local time. With the Mars Atmosphere and Volatile Evolution (MAVEN) mission, we are now able to extend this analysis to a larger range of altitudes and local times. Here we use electron PADs measured using the Solar Wind Electrostatic Analyzer and Magnetometer instruments on MAVEN to analyze the magnetic topology of the nightside Martian environment. We use several characteristic PAD shapes to determine where Martian magnetic field lines are open or closed to the solar wind and present frequency maps of how these PAD shapes vary both geographically and with altitude. Finally, we present an initial analysis of the variation of the PAD shapes with local time, finding that trapped electron distributions become increasingly frequent as crustal fields rotate from dusk to dawn across the nightside of Mars.

1. Introduction

Because Mars lacks a global dynamo, the interplanetary magnetic field (IMF) carried by the solar wind is able to directly interact with the planet's ionosphere. As the IMF drapes around the planet, it forms an induced magnetosphere similar to those of other unmagnetized bodes in the solar system. The Martian system is uniquely complex, though, due to the presence of crustal magnetic fields. Scattered in clusters across the planet's surface are pockets of crustal magnetism, remnant from when the planet possessed a global magnetic field (Acuna et al., 1999). As the IMF encounters Mars, it interacts with these crustal magnetic fields to produce an intricate topological system. In some areas, the crustal magnetic field lines reconnect with the IMF to produce lines of connectivity between the planet and the solar wind, while in other areas they are unaffected and act as small-scale magnetic shields. Because of this, energetic inputs from the solar wind (such as auroral heating) can often be restricted to localized regions of the Martian atmosphere. This in turn means that variations in magnetic topology can affect particle escape and over time may have influenced the planet's evolution.

The energization and outflow of charged particles at Mars is inherently dependent on the magnetic field environment. Low-energy ions and electrons will travel along magnetic field lines much more readily than across them, meaning that the local magnetic field acts as a direct determinant of the path of ionspheric particles. Atmospheric ion outflow can therefore be locally suppressed or enhanced depending on where magnetic fields are providing an avenue of escape. Ergun et al. (2016) demonstrated that high-electron temperatures observed in the ionosphere could cause significant fluxes of ambipolar ion escape and that this escape is enhanced by nearly an order of magnitude in regions of vertical open field topology. Just as importantly, the deposition of solar wind energy into the Martian atmosphere is also guided by magnetic fields. On the nightside of Mars, superthermal electron flux acts as a dominant source of energy input (Fox et al., 1993). These electrons precipitate into the Martian atmosphere along the IMF and impart their energy as they collide with the atmosphere, ionizing and heating particles (Leblanc et al., 2008; Lillis et al., 2009).

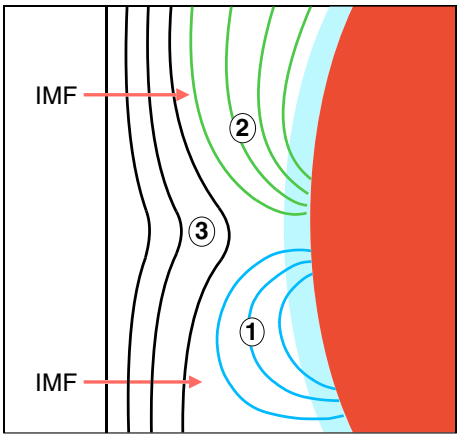

Figure 1. A simplified diagram of possible magnetic field topologies in the Martian environment. In this study, a magnetic field line is defined as being (1) closed if it is connected to the atmosphere at both ends, (2) open if it is connected to both the Martian atmosphere and the IMF, or (3) unconnected if it is only connected to the IMF.

The previously mentioned crustal magnetic fields add an extra layer of complexity. First discovered and mapped by Mars Global Surveyor (MGS), these magnetic fields have since been shown to frequently reconnect with the IMF as well as periodically form detached magnetic loops that flow away from Mars (Brain et al., 2010; Eastwood et al., 2008). Because magnetic field lines at Mars can serve as direct paths for both energy inflow and particle escape, it is important to characterize where and under what conditions magnetic fields do or do not connect to the IMF.

Magnetic fields at Mars are typically considered to have three possible field topologies: (1) closed, where the field line is connected at both ends to Mars; (2) open, where the field line is connected to Mars at one end and to the IMF at the other; or (3) unconnected (or "draped"), where the field line is solely connected to the IMF (Bertucci et al., 2003; Brain et al., 2007; Nagy et al., 2004). Figure 1 illustrates these possible configurations, labeled as 1, 2, and 3, respectively. In this study we are most interested in solar wind interactions with the Martian atmosphere, so here we define closed and open field lines through their connection to the atmosphere rather than to the planet's surface. For the same reason, we also do not analyze draped field lines within this study.

Distinguishing between these configurations, however, can prove difficult. Spacecraft measurements of magnetic field provide only a local magnetic field vector, giving no information on how that magnetic field behaves far from the spacecraft. For this reason, determination of magnetic topology requires the use of particle data in addition to magnetic field measurements. One such method is the use of electron energy spectra to determine the source of a measured electron population. Ionospheric and solar wind plasma each carry a characteristic electron energy signature, and the identification of these signatures can reveal the regions to which a magnetic field line is connected. This method has been used previously to identify high-altitude open field lines carrying atmospheric particles out into the Martian magnetotail (Frahm et al., 2006) as well as open fields connected to crustal structures allowing the entrance of high-energy solar wind electrons (Dubinin et al., 2008; Mitchell et al., 2001). This method is also used to map magnetic topology in a recent study by Xu et al. (2017); the results of which will be discussed more in later sections.

A separate method of identifying magnetic field topology involves the use of electron pitch angle distributions (PADs) to determine the ways in which directional electron flux has been altered along a measured field line (this method is detailed in section 2). Pitch angle distributions are frequently used to analyze the topology of the IMF as it flows through the solar system (e.g., Larson et al., 1997; Gosling et al., 2001) and were previously used to study magnetic topology at Mars by Brain et al. (2007). That study used electron PADs calculated by MGS to create a series of maps describing variations in magnetic topology across the surface of Mars. From these maps, it was determined that the strong crustal field complexes in the southern hemisphere are dominated by closed field topology everywhere except for small cusps located between the crustal loops and that the weakly magnetized northern hemisphere of Mars is dominated by open and draped topologies. However, the analyses presented in this study were limited in several important ways. First, the orbit of MGS only allowed for sampling at 2 a.m. and 2 p.m. local time. The rotation of the planet still allowed for complete coverage of the Martian surface and crustal fields, but field lines are likely to transition between open and closed as they move through different local times, a feature that MGS was unable to study. Second, the analysis was only performed for data in a narrow range of altitudes centered on 400 km. This provides a consistent baseline to work with, but an accurate description of Martian topology requires analysis across many altitudes. Draped field lines located at 400 km might rest directly above open or closed field lines (as in Figure 1), information that would be missed by MGS.

In the study presented here we use Mars Atmosphere and Volatile Evolution (MAVEN) data to address these limitations, expanding upon the work of Brain et al. (2007). We use data from across the Martian nightside to analyze geographic distributions of magnetic topology, and we present a first analysis of how pitch angle distributions vary with local time on the nightside of Mars. While the nightside environment can be characterized quite accurately through the use of pitch angle distributions, dayside analysis is made complicated by the presence of active photoelectron production. This can often isotropize PADs, drowning out many topological PAD signatures. Characterization of dayside topology using PADs is therefore left to a more dedicated future study. Additionally, the dayside regime is where the electron energy spectra method of Xu et al. (2017)

is most accurate, and in future works these two methods will be combined to create a full analysis of Martian magnetic topology.

In section 2 of this study we present descriptions of the data products used and our method of processing PAD distributions. In section 3 we describe how PADs are used to infer magnetic topology. In section 4 we present a case study illustrating our interpretation of PAD signatures. In section 5 we compare overall PAD statistics to those reported by the MGS spacecraft. In section 6 we present maps of how these PAD shapes vary geographically and with altitude. In section 7, we present an initial analysis of local time variations across the nightside of Mars. In section 8, we summarize these results and suggest areas of future study that would improve our understanding of the Martian magnetic environment.

2. Description of Instrument and PAD Shapes

The primary data product used in this study is that of electron pitch angle distributions measured using the Solar Wind Electron Analyzer (SWEA) and Magnetometer (MAG) instruments on MAVEN (Connerney et al., 2015; Mitchell et al., 2016). SWEA is a hemispheric electrostatic analyzer designed to measure both solar wind electrons and ionospheric photoelectrons at Mars across a series of energies spanning 3 eV to 4.6 keV. The instrument field of view covers 360° in azimuth with 22.5° resolution and 120° in elevation with 20° resolution. The electron energy flux distributions measured by SWEA are paired with magnetic field vectors measured by the Magnetometer (MAG) to produce a PAD every 2 s. Due to the large instrument field of view, SWEA generally samples a wide range of angles relative to the magnetic field direction. This means that the resulting PADs generally are able to cover the complete range of pitch angles, from 0° (parallel to the magnetic field) to 180° (antiparallel). When the magnetic field direction is close to SWEA's axis of symmetry, the PAD range is narrower (a minimum range of 120° resulting when the magnetic field points directly along this axis). The data used in this study were collected between 10 October 2014 and 24 March 2017, spanning slightly over one Martian year. Over this time, MAVEN's orbit continually precessed, with its periapsis location progressing across the dawnside, duskside, dayside, and nightside. Though MAVEN's elliptical orbit samples altitudes up to ~6,000 km, in this study we are primarily interested in magnetic topology near the ionosphere and so only consider data taken below 500 km. Additionally, this study is restricted to the nightside of Mars, only using data taken within the geometric shadow of the planet.

The general method used in this study is to determine the topology of the magnetic fields observed by MAG through analysis of the PAD signatures measured by SWEA. To accomplish this, 800,000 PADs were analyzed and labeled as corresponding to distinct PAD shapes. Here we use PADs measured for 100–300 eV electrons. This energy range is chosen both because it effectively targets the shocked incoming solar wind particles that are expected to dominate the nightside and because it is directly comparable to the 115 eV PADs used by Brain et al. (2007). In order to increase the counting statistics of our electron fluxes, groups of four consecutive PADs were coadded. For each measured angle, the electron energy fluxes of these four PADs were summed, and their corresponding errors were propagated. Groups of four were chosen so as to give reasonably large flux counts without decreasing the spatial resolution too drastically. We found that coadding in this way allowed for the most robust identification of PAD shapes, and we verified that the results do not change appreciably when using individual PADs or groups of two instead. In these cases, the statistical trends presented in this paper remained the same, with observation frequencies changing by only 5–10 percentage points. Coadding in this way produced 200,000 coadded PADs, each corresponding to 8 s of measurement. Every distribution was then separated into a downward component and an upward component using the measured direction of the magnetic field. These components were labeled individually according to the relative fluxes of electrons traveling parallel and perpendicular to the magnetic field, as compared to the error (σ) associated with the measured electron flux. The four possible classifications are as follows:

1. Parallel flux is 2σ greater than perpendicular flux (field-aligned beam).
2. Parallel flux is 2σ lower than perpendicular flux (loss cone).
3. Parallel flux and perpendicular flux are within 2σ (isotropic).
4. Parallel and perpendicular flux are within 2σ but flux at intermediate pitch angles (40°-50°) is 2σ greater than perpendicular flux (conic).

Combining a PAD's four possible upward and four possible downward signatures results in 16 possible unique PAD signatures, a selection of which is shown in Figure 2. One final signature is the "electron depletion"

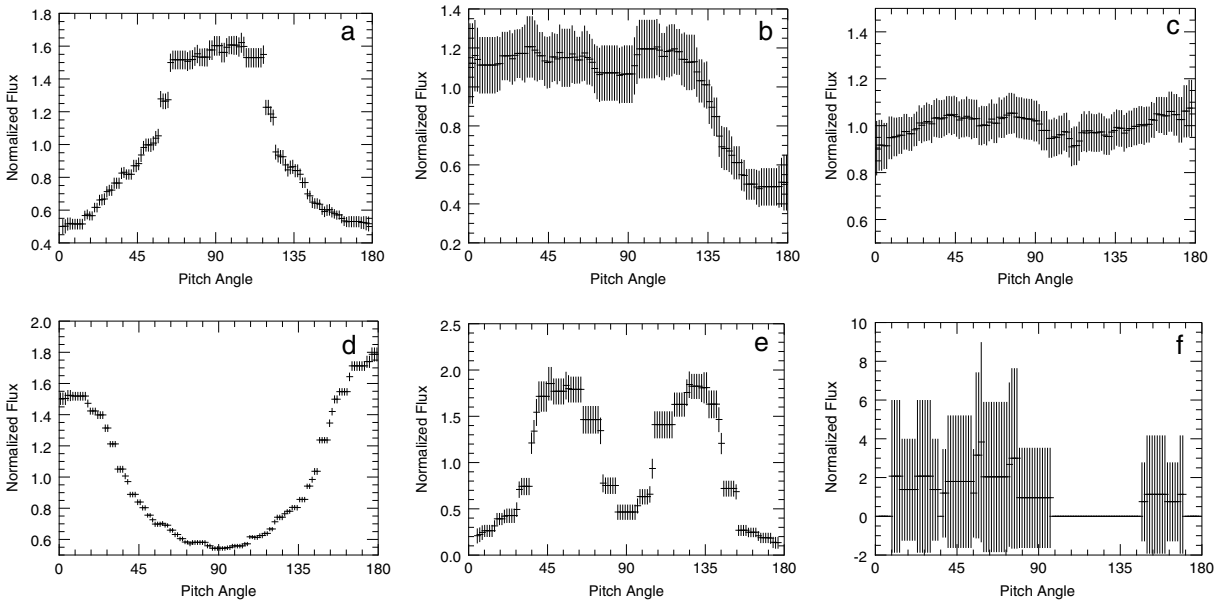

Figure 2. A selection of PAD signatures that are observed by SWEA. In order: (a) two-sided loss cone, (b) one-sided loss cone, (c) fully isotropic, (d) double field-aligned beam, (e) conic, and (f) electron depletion. The vertical lines represent 2σ error bars as calculated from the measured electron fluxes using Poisson statistics. Each PAD shown here is normalized such that the average flux is equal to 1.

(Figure 2f), in which the electron flux is within 2σ of zero in all directions. This signature represents a large depletion in superthermal electron flux, the implications of which are discussed later. Out of the 200,000 PADs, ~10,000 were excluded due to having either no usable data below 20° pitch angle or no usable data above 160° pitch angle. When this occurs, it is usually due to the spacecraft blocking a large section of SWEA's field of view. For the rest of the PADs, a successful match was found to one of our PAD signatures. In the following sections, we discuss the interpretation of these different PADs, first describing how PAD shapes are used to infer magnetic topology and then providing a case study to illustrate these inferences.

3. Interpretation of Pitch Angle Distributions

Open field lines (labeled "2" in Figure 1) are those that are connected both to the Martian atmosphere and the IMF. These lines provide a region of interaction between solar wind particles and the ionosphere, and it is through this interaction that we are able to easily identify the open lines with PADs. As electrons travel downward toward Mars along an open field line, they encounter stronger magnetic fields as the field lines converge. Through conservation of the first adiabatic invariant, these electrons eventually mirror, reflecting back upward once the magnetic field strength becomes sufficiently large. However, the location of this mirror point varies based on electron pitch angle. Particles moving more directly along the field line are able to travel farther down into the Martian atmosphere before mirroring and in doing so are more likely to be absorbed by the collisional atmosphere and lost. This results in a PAD depleted in upward returning field-aligned flux, otherwise known as a one-sided loss cone (Figure 2b). To identify open field lines, we therefore search for PADs in which the downward flux is either isotropic or field aligned and the upward flux contains a loss cone. Example observations of these loss cones are shown in the case study that is presented in the next section. One-sided loss cones have been studied previously at Mars for the purposes of mapping the Martian crustal fields (Mitchell et al., 2007), inferring magnetic topology (Brain et al., 2007) and estimating neutral atmosphere densities (Lillis et al., 2005).

Closed magnetic field lines (labeled "1" in Figure 1) are loops of magnetic field connected to the Martian atmosphere at both ends (foot points). Depending on whether these foot points are located on the dayside or nightside of Mars, closed loops can exhibit a variety of PAD signatures. In this study we only consider the signatures that are produced when both foot points are located on the nightside of the planet: electron depletions (Figure 2f) and two-sided loss cones (Figure 2a).

Electron depletions are large reductions in superthermal electron flux on the nightside of Mars that were first observed by MGS and have since been investigated by several authors (Dubinin et al., 2008; Lillis & Brain, 2013; Mitchell et al., 2001; Steckiewicz et al., 2015; Shane et al., 2016). These depletions are due to the presence of closed loops of magnetic field that have lost their associated electron population through recombination with the atmosphere. While on the dayside of Mars, these loops are filled with plasma due to the presence of significant photoionization, but after rotating to the nightside this electron source process is lost, and the loss process of atmospheric absorption dominates. Because electron depletions are robust trackers of closed field lines, we identify them in the PAD analysis presented here, defining depletions as those PADs that have flux rates that are statistically zero across all pitch angles.

Two sided loss cones (also referred to as trapped distributions) result from electrons adiabatically mirroring between regions of increased magnetic field strength. As electrons travel along closed magnetic field loops and move to lower altitudes, they encounter stronger magnetic fields and are reflected back upward in the same manner as on open field lines. But unlike on open field lines, these particles then travel along the loop to the other foot point and reflect once more, creating a population of trapped, mirroring electrons. As discussed previously, particles moving more directly along the field (i.e., pitch angles near 0° or 180°) travel lower in altitude before mirroring and thus are more likely to be lost. This leads to a PAD that exhibits a loss cone in both the parallel and antiparallel direction. Two-sided loss cones have been extensively studied for particles trapped within the Earth's magnetosphere (Abel & Thorne, 1998; Lyons et al., 1972; West et al., 1973), and have previously been used at Mars to infer closed field topology (Brain et al., 2007; Lillis et al., 2009) as well as to estimate low-altitude magnetic field strength (Mitchell et al., 2007; Lillis et al., 2008).

It is important to note here that cross-terminator closed field lines, containing one foot point on the dayside and one foot point on the nightside, can often be mistaken for open field lines with the analysis method used in this study. As photoelectrons from the dayside travel to the nightside, they can be mirrored or absorbed, producing the same one-sided loss cone signature as open field lines. This photoelectron signal is often too weak in the 100–300 eV energy range to affect our analysis, but it is still a source of error (particularly near the terminator) that should be recognized throughout this study.

4. Case Study

Figure 3 contains data taken during an inbound pass deep on the nightside of Mars, throughout which a variety of PAD signatures are observed. This orbit reaches periapsis at an altitude of 152 km and a solar zenith angle of 178°. A comparison between the measured and modeled magnetic fields shows that the modeled crustal field contribution (Cain et al., 2003) matches the measurements almost exactly. This suggests that the magnetic fields here are dominated by crustal sources. On panels 3 and 4 are plotted electron fluxes and PADs obtained by SWEA, and the observations are divided into three time periods that show distinct PAD shapes. At the start of time period 1, a clear conic signature is present. Conical PADs were studied in detail by Ulusen et al. (2011), who proposed that they may be formed through the merging of neighboring open field lines, forming new closed loops. However, these signatures are rare enough (<1%) that they are ignored in this study. Here the conic quickly transitions into a trapped distribution, indicating closed field topology. Transitioning to time period 2, SWEA begins to measure consistent one-sided loss cones, characterized by a strong depletion in field-aligned flux away from the planet. This suggests that the crustal fields being sampled here are connected to the IMF. The strong radial magnetic field component observed until 04:39 suggests that MAVEN is sampling a cusp between crustal field structures. After this point the field is directed more horizontally, but the one-sided loss cones remain, suggesting that MAVEN has likely transitioned to measuring the upper section of a weaker crustal field structure that is also open to the solar wind. This signature abruptly vanishes at 04:41, with the total electron flux dropping to near zero and remaining there. This extended electron depletion suggests that MAVEN is passing deep within closed nightside crustal fields. Here there is no solar wind input, and any trapped ionospheric population from the dayside has decayed away due to atmospheric absorption. At brief intervals we observe spikes in the electron flux, such as at 04:43 or just before 04:47. These have been observed previously (Mitchell et al., 2001) and are generally taken to indicate small pockets of open magnetic field located between closed crustal structures. Here the flux spikes between 04:42 and 04:44 do not contain enough 100–300 eV electrons to be recognized by our PAD processing, but the spike at 04:47 produces a brief loss cone signature, with electron flux extending slightly past 90° pitch angle. This allows us to identify it as open to the solar wind.

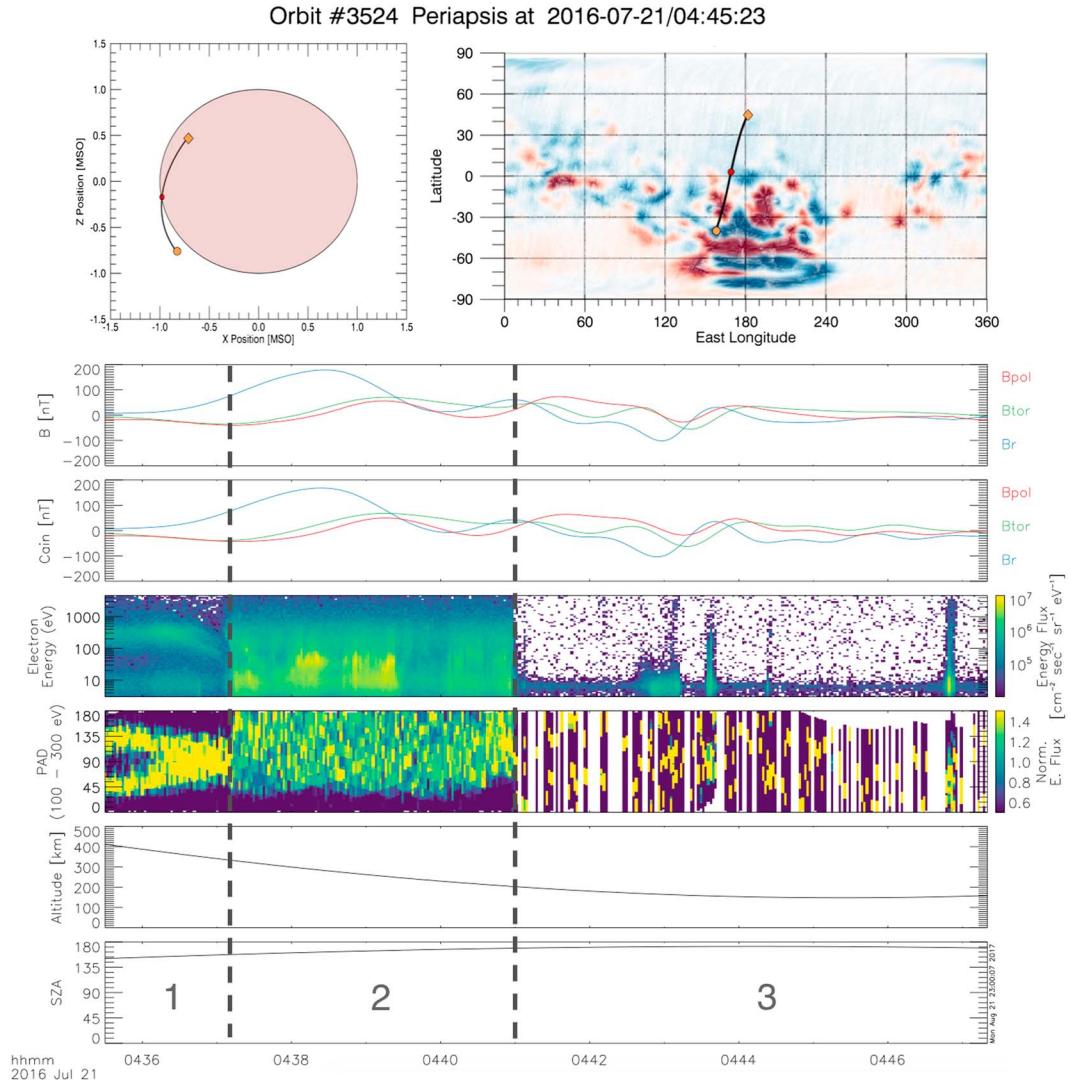

Figure 3. Inbound pass of MAVEN located deep on the nightside of Mars. The orbit trajectories shown in the upper panels are capped at an altitude of 500 km, with inbound marked by an orange circle, outbound an orange diamond, and periapsis a red circle. The upper right panel contains a map of radial crustal field strength measured by MGS, as shown in Brain et al. (2003). The instrument data panels show, in order from top to bottom, (1) magnetic field vector shown in spherical coordinates (Br = radial, Btor = toroidal [ϕ], Bpol = poloidal [θ]), (2) modeled crustal magnetic field contribution from the Cain model (Cain et al., 2003), (3) electron energy spectrogram in units of energy flux, (4) pitch angle distributions of 100–300 eV electrons, with each measurement normalized by its mean value, (6) MAVEN's altitude, and (7) solar zenith angle.

5. Comparison to Mars Global Surveyor Results

Before studying the full distribution of field topologies across the nightside, it is useful to first make a comparison to the results obtained by Brain et al. (2007). Here we limit our MAVEN data to the region of space that was sampled by MGS, allowing us to directly compare PAD observation frequencies as an initial check for consistency. This is shown in Table 1, which contains the relative occurrence rates for a variety of PAD shapes. For each shape, two numbers are shown. These represent the percentage of PADs on the nightside of Mars that exhibit the corresponding shape, as measured by MAVEN and by MGS, respectively. The MGS results are as reported in Brain et al. (2007), and the MAVEN results only use data taken between 1 and 3 h local time and 350–450 km altitude.

While the observation frequencies reported by MAVEN and MGS for each PAD are not entirely equivalent, the overall trends shown are comparable. The most commonly identified PAD shape is an incident isotropic

Table 1
Percentage of 100–300 eV PADs With the Given PAD Distribution

	Incident PAD signature				
Returning PAD signature	Isotropic	Loss cone	Beam	Conic	Depletion
Isotropic	19.8 / 8.8	4.6 / 1.1	5.4 / 3.4	1.3 / 0.3	-
Loss Cone	25.7 / 23.1	11.8 / 12.8	4.4 / 7.5	0.9 / 0.4	-
Beam	0.6 / 0.6	0.1 / 0.2	1.3 / 2.8	0.5 / 0.2	-
Conic	0.4 / 0.8	0.2 / 0.3	1.9 / 3.9	1.3 / 1.4	-
Depletion	-	-	-	-	17.0 / 31.5

Note. The percentages in each cell represent MAVEN observations and MGS observations, respectively. MAVEN data were limited to 350–450 km and 1–3 local time for the purpose of comparison to MGS's mapping orbit. MGS statistics are taken from Brain et al. (2007).

distribution with a loss cone in the return flux, generally indicative of open field lines. These account for ~25% of all observations. Two-sided loss cones are also fairly dominant, accounting for 12% of MAVEN PAD measurements and 12.8% of MGS PAD measurements. As discussed before, these PADs usually represent particles mirroring within closed field topology. One large difference between the results of Brain et al. (2007) and those presented here is the decreased likelihood of measuring electron depletions. While MGS observed electron depletion PADs 31.5% of the time, MAVEN encounters them only ~17% of the time while near 2 a.m. and 400 km. This discrepancy is mainly due to two factors. First, MAVEN's sampling near 2 a.m. local time has not covered all geographic locations equally, with a greater number of PADs sampled in the Mars' northern hemisphere. This means that the largest crustal field complexes (located in the southern hemisphere) were sampled less frequently, leading to comparatively small frequency of observing electron depletions. Additionally, the increased accuracy of the SWEA instrument when compared to MAG/ER means that fewer PADs are found to have fluxes that are statistically equal to zero. This causes some PADs that would have been identified as electron depletions to instead be labeled as isotropic distributions with low count rates. For this reason, MAVEN has also observed fully isotropic distributions much more frequently than MGS, with these accounting for ~20% of observations rather than 8.8% of observations.

6. Statistical Maps

6.1. Open Field Lines

Brain et al. (2007) presented maps of one-sided loss cone measurements using MGS data taken at 400 km, 2 a.m. local time. With these maps they showed that open field lines are found across the nightside at all geographic locations that are not dominated by crustal fields. Here we explore this result further, extending the analysis through the larger parameter space covered by MAVEN.

Figure 4a is a geographic map of one-sided loss frequency, using all MAVEN data taken below 500 km on the nightside of Mars. The color in each bin represents the fraction of PADs measured in that bin that exhibited a loss cone in upward electron flux. Overlayed on the map are contours of radial crustal magnetic field strength (20 and 40 nT) as measured at 400 km by MGS. Throughout the strong crustal fields in the southern hemisphere, one-sided loss cones are relatively infrequent. This implies that the crustal fields, as would be expected, are rarely open to the solar wind. However, in the regions where crustal fields are directed most radially (the center of the contours), one-sided loss cones are observed very frequently, approaching 50% of observations. In this way we can see that these crustal cusp regions are frequently open to the solar wind, acting as narrow windows of connectivity among the crustal complexes.

Across the noncrustal regions, such as the weakly magnetized northern hemisphere, loss cones are more uniformly common. As discussed in Brain et al. (2007), these loss cones, while indicative of open field lines, do not necessarily suggest a connection to crustal sources. Rather, this signature could also be produced by draped lines of IMF that intersect the Martian atmosphere, with absorption and scattering producing a depletion in return flux. In regions of weak crustal magnetization, it is likely that both configurations are present, and in most respects they carry the same implications. In both situations the solar wind can interact with the Martian atmosphere to deposit energy or guide ion escape, though the interaction might penetrate deeper when there are crustal sources guiding the field lines down toward the planet.

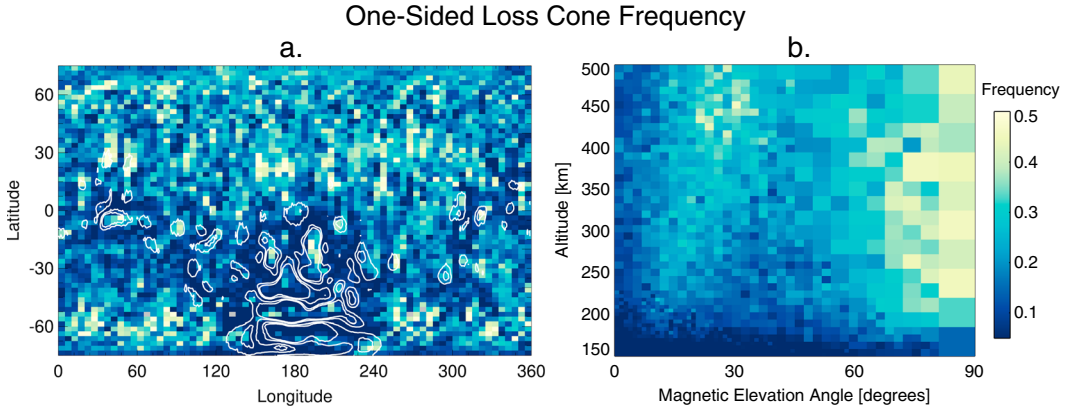

Figure 4. (a) Geographic distribution of one-sided loss cones on the nightside of Mars below 500 km. The bins are 2.5° by 2.5°, and the color in each bin represents the fraction of PADs measured within that bin that were identified as containing loss cones. "Nightside" is here taken to mean the geometric shadow of the planet. Contour lines of MGS inferred radial crustal magnetic field strength of 20 and 40 nT at 400 km are included (Connerney et al., 2001). (b) Observation frequency on the nightside as a function of altitude and magnetic elevation angle. Color bar applies to both figures.

This is explored more in Figure 4b, which shows nightside open field line frequency as a function of altitude and magnetic elevation angle. Here 0° represents horizontal and 90° represents vertical with respect to the surface of the planet. Once again, bin coloration represents the fraction of PADs identified as one-sided loss cones, and here the bin size varies with data density such that each bin contains at least 100 data points. In this figure we can see two distinct favored orientations for open field lines. First, vertically oriented fields appear to display open topology at a relatively enhanced frequency. When these vertical fields extend to low altitudes (below ~300 km), as they would in a crustal cusp, loss cones become particularly frequent, accounting for roughly 50% of observations. Second, one-sided loss cones are also found at low magnetic elevation angles but more commonly when these fields are located at higher altitudes (above ~400 km). This population of observed loss cones likely represents open field lines threading through the nightside atmosphere. At lower altitudes, a greater portion of horizontal fields are crustally sourced and closed to the solar wind. This leads to fewer measurements of one-sided loss cones. Interestingly, there appears to be a distinct minimum in loss cone frequency at the midrange elevation angles between 40° and 60°. Open field lines are much more dominant in vertical crustal cusps and horizontal lines of draping IMF.

Nightside open field lines were also mapped by Xu et al. (2017) through the identification of characteristic energy spectra. That study also found open field lines to be consistently present across the northern hemisphere but at an overall lower frequency than we find here (20% of measurements as compared to 40%). Additionally, the open field lines that we identify throughout crustal field cusps are not reflected in Xu et al. (2017). This is due to the open field identification method of that work requiring the presence of photoelectrons. Open field lines that connect directly to the nightside of Mars contain no photoelectrons and are therefore labeled as "draped" in their study, while those open fields that connect to the dayside of the planet are correctly classified.

6.2. Closed Field Lines—Electron Depletions

The distribution of observed electron depletions is explored in Figures 5a and 5b. Figure 5a shows a geographic map of electron depletion frequency for all PADs measured below 500 km on the nightside of the planet. As expected, electron depletions are most commonly found in and around crustal field structures and seem to be most dominant near the inner sections of the crustal field arcades. This agrees with the previous results of Brain et al. (2007) at 400 km, as well as those of Steckiewicz et al. (2015), who studied decreases in electron fluxes in three different energy ranges measured by SWEA to analyze electron depletions in the northern hemisphere of Mars. With this geographic distribution in mind, Figure 5b explores the altitude dependence of electron depletions. Plotted here is the frequency of observing electron depletions on the nightside as a function of altitude and crustal field strength. Crustal field strength is inferred using the Cain model of crustal fields (Cain et al., 2003). A trend can be immediately identified, with electron depletions measured more frequently at lower altitudes and in stronger crustal fields. Within the strongest crustal fields,

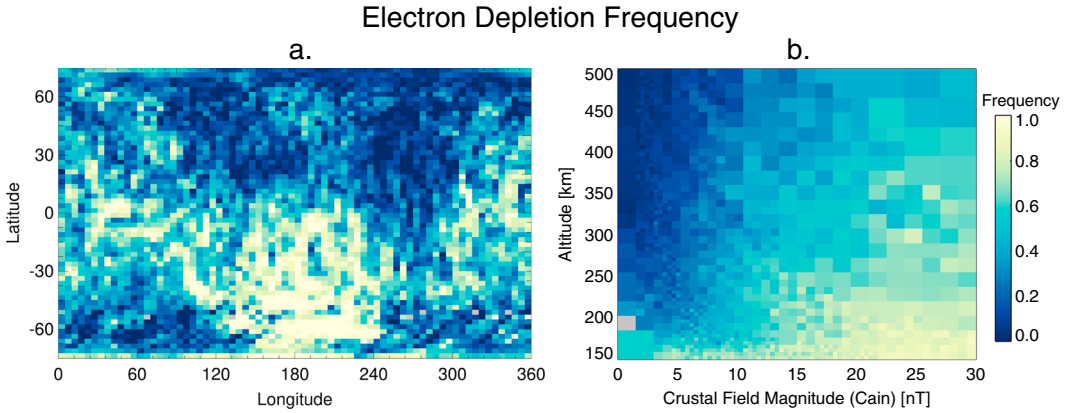

Figure 5. (a) Geographic distribution of electron depletions on the nightside of Mars below 500 km altitude. The bins are 2.5° by 2.5°, and the color in each bin represents the fraction of PADs measured within that bin that were identified as depletions. "Nightside" is taken to mean the geometric shadow of the planet. (b) Observation frequency as a function of altitude and modeled crustal field strength at the point of measurement (Cain model). Color bar applies to both figures.

electron depletions account for nearly 100% of measurements. Additionally, one can see here that at the lowest altitudes electron depletions dominate even in regions of weak crustal field strength. As discussed in Steckiewicz et al. (2015), this indicates the upper boundary of the collisional atmosphere, where the electrons are lost due to CO_2 absorption regardless of their magnetic environment. Electron depletions were also mapped by Xu et al. (2017), and the observation frequencies shown here agree very well with the results of that study.

6.3. Closed Field Lines—Two-Sided Loss Cones

A geographic map of trapped distributions is shown in Figure 6a. Once again this map includes all PADs measured below 500 km on the nightside of Mars. Like electron depletions, trapped PAD signatures are expected to indicate closed field lines. As such they are also seen to occur more frequently near crustal magnetic sources, with almost no trapped distributions found in the weakly magnetized sections of the northern hemisphere. But unlike electron depletions, two-sided loss cones are preferentially located around the edges of crustal field structures. In the centermost sections of the large crustal field complexes, trapped distributions are almost entirely absent, but near the more weakly magnetized perimeters they are found frequently. We also observe that trapped distributions are especially common in an area near 140° E, 70° S, as was reported in Brain et al. (2007). Based on the study of Lillis and Brain (2013), it seems that this region also experiences consistently large fluxes of electron precipitation regardless of upstream solar wind conditions. The exact reason

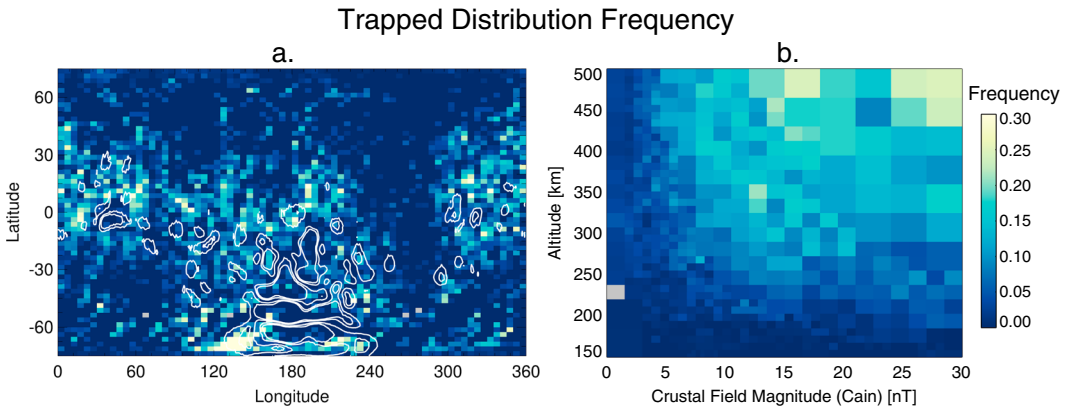

Figure 6. (a) Geographic distribution of two-sided loss cones on the nightside of Mars below 500 km. The bins are 2.5° by 2.5°, and the color in each bin represents the fraction of PADs measured within that bin that were identified as two-sided loss cones. Nightside is here taken to mean the geometric shadow of the planet. Contour lines of MGS inferred radial crustal magnetic field strength of 20 and 40 nT at 400 km are included. (b) Observation frequency as a function of altitude and modeled crustal field strength at the point of measurement (Cain model). Color bar applies to both figures.

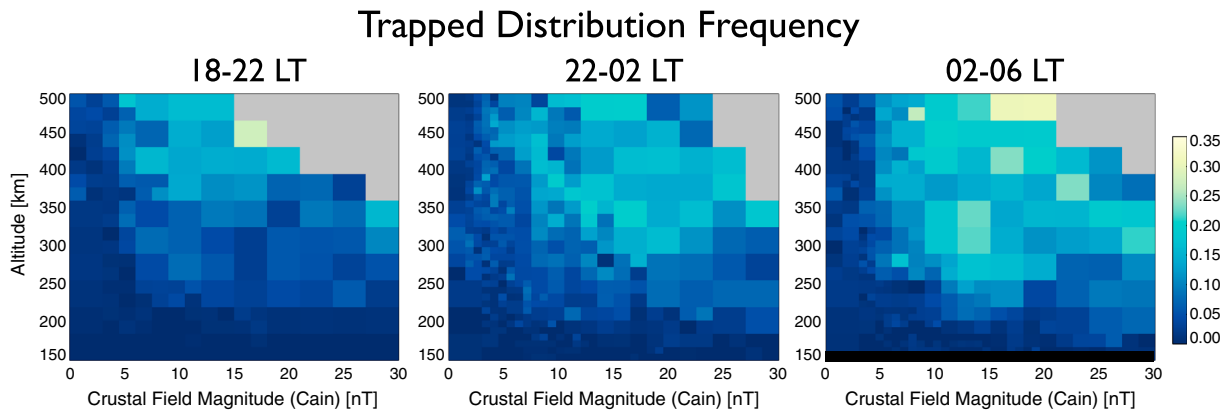

Figure 7. Observation frequencies of two-sided loss cones are shown as a function of altitude and modeled crustal field strength for three local time divisions. The color in each bin represents the fraction of PADs measured within that bin that were identified as two-sided loss cones. Gray is used for bins without an adequate number of data points (<50). Only observations made within Mars' shadow are included here. Color bar is shared between all panels.

for this is not fully understood, but it is likely that the trapped distributions shown here are sourced from this enhanced electron precipitation.

We can investigate the altitude dependence of trapped distributions more fully with Figure 6b, which shows trapped distribution frequency as a function of altitude and crustal field strength. Here we can see that trapped distributions are found more commonly within strong crustal fields and at high altitudes. In this way, trapped distributions and electron depletions complement each other. Both are indicative of the closed topology found in crustal field loops, but while electron depletions dominate the enclosed low-altitude sections, trapped populations fill the high-altitude outer edges of the loops. This confirms a commonly held picture of closed field lines on the nightside of Mars. The outer sections of crustal fields are populated with mirroring electrons that are likely supplied either through the recent closing of field lines by magnetic reconnection or through inward diffusion from the surrounding crustal cusps that are open to the solar wind. The inner layers are meanwhile significantly depleted, having lost much of their associated plasma population to atmospheric collisions. This was previously illustrated in Brain et al. (2007) using MGS data at 400 km and 2 a.m. local time. Here we have extended the analysis to show that the trend holds for data across the nightside of Mars.

7. Local Time Variations of Trapped Distributions

In addition to studying the frequency of PAD signatures across the nightside of Mars as a whole, MAVEN provides us with the opportunity to further analyze how these PAD frequencies vary with local time. Because MGS's mapping orbit was limited to 2 a.m./2 p.m. local time, Brain et al. (2007) were never able to address how magnetic fields at Mars might experience topological changes as they rotate around the planet. Here we can start to study this possibility. Continuing directly from the previous section, we focus our analysis on how trapped electron signatures vary with local time on the nightside of Mars.

While MAVEN's orbital progression has provided for data across all local times at Mars, the geographic and altitude coverage at each local time has varied greatly. Because we know that PAD shapes are strongly influenced by the crustal field environment, this means that we could encounter strong observational biases when separating our data. We therefore analyze the data in the manner of Figure 7, which explores how the frequency of observing trapped distributions on the nightside of Mars changes from dusk to dawn. Once again only considering data taken in the planet's shadow, we break our analysis into three sections of local time. For each local time segment, we map the observation frequency as a function of altitude and crustal field magnitude. Though the exact regions sampled to produce each panel may be different, dividing the data in this way allows us to remove the crustal field sampling biases present between local times.

In each of the three panels, the general trend in where trapped signatures are observed remains constant, with a higher observation frequency at higher altitudes and in strong crustal fields. However, moving from dusk (18 LT) to dawn (06 LT), the total occurrence rate of trapped PADs increases across all altitudes. At 200 km

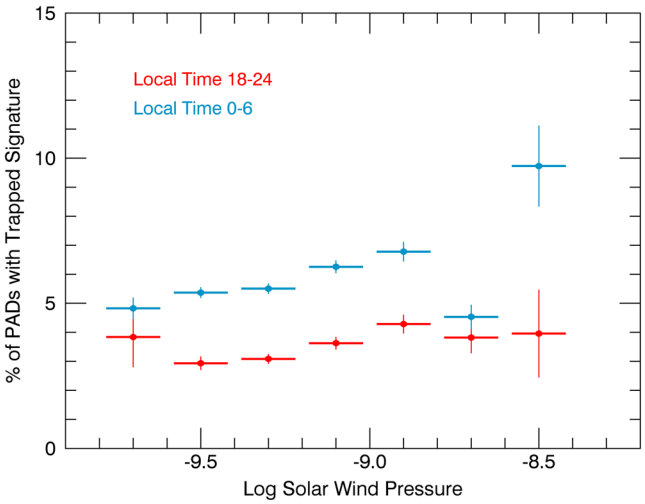

Figure 8. Percentage of observed PADs on the nightside of Mars showing a trapped signature during different upstream solar wind strengths. Only observations made near crustal fields (Cain model Strength >5 nT) and below 500 km were included in this figure.

altitude this is an increase in frequency from ~0.05 to ~0.15, while at 400 km it is an increase from a frequency of ~ 0.15 to ~0.25.

It is important to consider that the local time variations observed here might also be due to sampling biases present in the solar wind conditions. It is currently not well described how changes in the solar wind affect low-altitude topology at Mars, so we must account for the possibility that the upstream solar wind might have been very different when Maven sampled the dawnside of the planet as compared to the duskside. This is explored in Figure 8. Here we show the chance of observing a trapped distribution below 500 km on the nightside of Mars as a function of the strength of the upstream solar wind. Solar wind dynamic pressure was determined for each measured PAD using MAVEN measurements of the solar wind from earlier in the same orbit (Halekas et al., 2016). One representative value of solar wind pressure was taken for each orbit and applied to all the measurements made within that orbit. Orbits in which MAVEN did not sample the solar wind were excluded in making this figure. Because two-sided loss cones are essentially only relevant near crustal sources (see Figure 6), we also exclude PADs measured far from crustal fields (Cain Model Strength <5 nT). Two sets of data points are shown on the plot. Those in red represent data taken between 18 and 24 local time (the duskward half of Mars' nightside), while those in blue represent data taken between 0 and 6 local time (the dawnward half). Vertical error bars were calculated from a simplistic Poisson statistic, using the square root of the number of identified trapped PADs. Horizontal error bars represent the range of pressures used in calculating the corresponding percentage.

There are two main conclusions to be drawn from this figure. First, regardless of the incoming solar wind pressure, two-sided loss cones are found roughly twice as often on the dawnside of Mars as compared to the duskside. This confirms the result shown in Figure 7 and demonstrates that it is not due simply to a solar wind sampling bias. Second, it appears that the incoming solar wind pressure does cause variability in low-altitude PAD shapes, as the observation frequency of two-sided loss cones is not constant through the varied conditions. This is to be expected, as the magnetic topology across Mars is intrinsically dependent on interactions with the solar wind. However, there does not seem to be a straightforward trend present in the figure shown here (though a slight increase in trapped signature observations might be present at higher solar wind pressures). Solar wind drivers are likely to affect low-altitude magnetic topology in a complex manner deserving of its own study. As such, the specifics and implications are not discussed here and will rather be explored in a future work.

Thus far, we have not identified a definite cause of the observed local time variations. One possibility is that magnetic fields are more likely to have closed topology on the dawnward half of the nightside. This would be surprising but could conceivably be due to spatial differences in how reconnection processes are established in the Martian system. This possibility could be addressed through modeling studies. A second explanation could be that closed magnetic field loops become increasingly likely to contain trapped PADs rather than electron depletions as they rotate through the nightside. This could be due to a local time asymmetry in the electron precipitation that sources the trapped distributions, though the incoming electron flux is not expected to be higher near dawn.

8. Summary and Conclusion

We present a statistical analysis of electron pitch angle distributions calculated using the SWEA and MAG instruments aboard MAVEN. We use these pitch angle distributions to infer the magnetic topology below 500 km across the nightside of Mars. We find good agreement with previous results obtained by the MGS spacecraft at 400 km altitude and 2 a.m. local time and then extend this analysis to the broader range of altitudes sampled by MAVEN. We find that crustal sources on the nightside exhibit closed topology almost uniformly and are composed of an outer layer of mirroring particles that surround a core significantly depleted of electrons. Open field lines are found across the nightside in two favored configurations. They drape across all regions not dominated by crustal sources but only extend to the lowest altitudes consistently in the crustal cusps, where they descend directly vertically. We then present an analysis of local time variations in trapped

electron signatures. Two-sided loss cones become increasingly frequent as crustal magnetic field sources move from dusk toward dawn across the nightside of Mars. While we have not identified a physical explanation for this, we can confirm that the variation appears to be guided by local time, rather than due to any sampling bias. The work presented here serves both to confirm the results of previous studies, as well as to act as a foundation for future studies on how magnetic topology at Mars varies with upstream solar wind conditions. As MAVEN continues to collect PAD data, it is filling in an even more complete parameter space. Increased statistics at all local times, altitudes, geographic locations, and upstream conditions will allow for a better understanding of the topological dynamics in the Martian system. Through comparisons with other MAVEN data sets we should be able to quantify the effect that variations in magnetic topology have on particle outflow and energy transport.

Acknowledgments
MAVEN data used in this study are available through the NASA Planetary Data System.

References

Abel, B., & Thorne, R. M. (1998). Electron scattering loss in Earth's inner magnetosphere: 1. Dominant physical processes. *Journal of Geophysical Research*, *103*(A2), 2385–2396.

Acuna, M., Connerney, J., Lin, R., Mitchell, D., Carlson, C., McFadden, J., … Cloutier, P. (1999). Global distribution of crustal magnetization discovered by the Mars Global Surveyor MAG/ER experiment. *Science*, *284*(5415), 790–793.

Bertucci, C., Mazelle, C., Crider, D., Vignes, D., Acuña, M., Mitchell, D., … Winterhalter, D. (2003). Magnetic field draping enhancement at the Martian magnetic pileup boundary from Mars global surveyor observations. *Geophysical Research Letters*, *30*, 1099. https://doi.org/10.1029/2002GL015713

Brain, D., Bagenal, F., Acuña, M., & Connerney, J. (2003). Martian magnetic morphology: Contributions from the solar wind and crust. *Journal of Geophysical Research*, *108*, 1424. https://doi.org/10.1029/2002JA009482

Brain, D., Baker, A., Briggs, J., Eastwood, J., Halekas, J., & Phan, T.-D. (2010). Episodic detachment of Martian crustal magnetic fields leading to bulk atmospheric plasma escape. *Geophysical Research Letters*, *37*, L14108. https://doi.org/10.1029/2010GL043916

Brain, D., Lillis, R., Mitchell, D., Halekas, J., & Lin, R. (2007). Electron pitch angle distributions as indicators of magnetic field topology near Mars. *Journal of Geophysical Research*, *112*, A09201. https://doi.org/10.1029/2007JA012435

Cain, J. C., Ferguson, B. B., & Mozzoni, D. (2003). An $n = 90$ Internal potential function of the Martian crustal magnetic field. *Journal of Geophysical Research*, *108*, 5008. https://doi.org/10.1029/2000JE001487

Connerney, J., Acuna, M., Wasilewski, P., Kletetschka, G., Ness, N., Reme, H., … Mitchell, D. (2001). The global magnetic field of Mars and implications for crustal evolution. *Geophysical Research Letters*, *28*(21), 4015–4018.

Connerney, J., Espley, J., Lawton, P., Murphy, S., Odom, J., Oliversen, R., & Sheppard, D. (2015). The MAVEN magnetic field investigation. *Space Science Reviews*, *195*(1–4), 257–291.

Dubinin, E., Fraenz, M., Woch, J., Winnigham, J., Frahm, R., Lundin, R., & Barabash, S. (2008). Suprathermal electron fluxes on the nightside of Mars: ASPERA-3 observations. *Planetary and Space Science*, *56*(6), 846–851.

Eastwood, J., Brain, D., Halekas, J., Drake, J., Phan, T., Øieroset, M., … Acuña, M. (2008). Evidence for collisionless magnetic reconnection at Mars. *Geophysical Research Letters*, *35*, L02106. https://doi.org/10.1029/2007GL032289

Ergun, R., Andersson, L., Fowler, C., Woodson, A., Weber, T., Delory, G., … Jakosky, B. M. (2016). Enhanced O_2^+ loss at Mars due to an ambipolar electric field from electron heating. *Journal of Geophysical Research: Space Physics*, *121*, 4668–4678. https://doi.org/10.1002/2016JA022349

Fox, J. L., Brannon, J., & Porter, H. (1993). Upper limits to the nightside ionosphere of Mars. *Geophysical Research Letters*, *20*(13), 1339–1342.

Frahm, R., Winningham, J., Sharber, J., Scherrer, J., Jeffers, S., Coates, A., … Dierker, C. (2006). Carbon dioxide photoelectron energy peaks at Mars. *Icarus*, *182*(2), 371–382.

Gosling, J., Skoug, R., & Feldman, W. (2001). Solar wind electron halo depletions at 90 pitch angle. *Geophysical Research Letters*, *28*(22), 4155–4158.

Halekas, J., Ruhunusiri, S., Harada, Y., Collinson, G., Mitchell, D., Mazelle, C., … Jakosky, B. M. (2016). Structure, dynamics, and seasonal variability of the Mars-solar wind interaction: MAVEN solar wind ion analyzer in-flight performance and Science Results. *Journal of Geophysical Research: Space Physics*, *122*, 547–578. https://doi.org/10.1002/2016JA023167

Larson, D., Lin, R., McTiernan, J., McFadden, J., Ergun, R., McCarthy, M., … Mazur, J. (1997). Tracing the topology of the October 18–20, 1995, magnetic cloud with $\sim 0.1–10^2$ keV electrons. *Geophysical Research Letters*, *24*(15), 1911–1914.

Leblanc, F., Witasse, O., Lilensten, J., Frahm, R., Safaenili, A., Brain, D., … Lundin, R. (2008). Observations of aurorae by SPICAM ultraviolet spectrograph on board Mars Express: Simultaneous ASPERA-3 and MARSIS measurements. *Journal of Geophysical Research*, *113*, A08311. https://doi.org/10.1029/2008JA013033

Lillis, R. J., & Brain, D. A. (2013). Nightside electron precipitation at Mars: Geographic variability and dependence on solar wind conditions. *Journal of Geophysical Research: Space Physics*, *118*, 3546–3556. https://doi.org/10.1002/jgra.50171

Lillis, R., Engel, J., Mitchell, D., Brain, D., Lin, R., Bougher, S., & Acuña, M. (2005). Probing upper thermospheric neutral densities at Mars using electron reflectometry. *Geophysical Research Letters*, *32*, L23204. https://doi.org/10.1029/2005GL024337

Lillis, R. J., Fillingim, M. O., Peticolas, L. M., Brain, D. A., Lin, R. P., & Bougher, S. W. (2009). Nightside ionosphere of mars: Modeling the effects of crustal magnetic fields and electron pitch angle distributions on electron impact ionization. *Journal of Geophysical Research*, *114*, E11009. https://doi.org/10.1029/2009JE003379

Lillis, R. J., Frey, H. V., Manga, M., Mitchell, D. L., Lin, R. P., Acuña, M. H., & Bougher, S. W. (2008). An improved crustal magnetic field map of Mars from electron reflectometry: Highland volcano magmatic history and the end of the Martian dynamo. *Icarus*, *194*(2), 575–596.

Luhmann, J., Johnson, R., & Zhang, M. (1992). Evolutionary impact of sputtering of the Martian atmosphere by O^+ pickup ions. *Geophysical Research Letters*, *19*(21), 2151–2154.

Lyons, L. R., Thorne, R. M., & Kennel, C. F. (1972). Pitch-angle diffusion of radiation belt electrons within the plasmasphere. *Journal of Geophysical Research*, *77*(19), 3455–3474.

Mitchell, D., Lillis, R., Lin, R., Connerney, J., & Acuña, M. (2007). A global map of Mars' crustal magnetic field based on electron reflectometry. *Journal of Geophysical Research*, *112*, E01002. https://doi.org/10.1029/2005JE002564

Mitchell, D., Lin, R., Mazelle, C., Rème, H., Cloutier, P., Connerney, J., … Ness, N. (2001). Probing Mars' crustal magnetic field and ionosphere with the MGS Electron Reflectometer. *Journal of Geophysical Research*, *106*(E10), 23,419–23,427.

Mitchell, D., Mazelle, C., Sauvaud, J.-A., Thocaven, J.-J., Rouzaud, J., Fedorov, A., … Jakosky, B. M. (2016). The MAVEN solar wind electron analyzer. *Space Science Reviews*, *200*(1–4), 495–528.

Nagy, A., Winterhalter, D., Sauer, K., Cravens, T., Brecht, S., Mazelle, C., … Trotignon, J. G. (2004). The plasma environment of Mars. *Space Science Reviews*, *111*(1–2), 33–114.

Shane, A. D., Xu, S., Liemohn, M. W., & Mitchell, D. L. (2016). Mars nightside electrons over strong crustal fields. *Journal of Geophysical Research: Space Physics*, *121*, 3808–3823. https://doi.org/10.1002/2015JA021947

Steckiewicz, M., Mazelle, C., Garnier, P., André, N., Penou, E., Beth, A., … Jakosky, B. M. (2015). Altitude dependence of nightside Martian suprathermal electron depletions as revealed by MAVEN observations. *Geophysical Research Letters*, *42*, 8877–8884. https://doi.org/10.1002/2015GL065257

Ulusen, D., Brain, D. A., & Mitchell, D. L. (2011). Observation of conical electron distributions over Martian crustal magnetic fields. *Journal of Geophysical Research*, *116*, A07214. https://doi.org/10.1029/2010JA016217

West, H., Buck, R., & Walton, J. (1973). Electron pitch angle distributions throughout the magnetosphere as observed on Ogo 5. *Journal of Geophysical Research*, *78*(7), 1064–1081.

Xu, S., Mitchell, D., Liemohn, M., Fang, X., Ma, Y., Luhmann, J., … Jakosky, B. (2017). Martian low-altitude magnetic topology deduced from MAVEN/SWEA observations. *Journal of Geophysical Research: Space Physics*, *122*, 1831–1852. https://doi.org/10.1002/2016JA023467